Nanoscale
2016, Volume 8 Issue 13 Pages 7105-7112
http://dx.doi.org/10.1039/c5nr09018k
http://archimer.ifremer.fr/doc/00368/47954/

Nanoplasmonics tuned “click chemistry”

Tijunelyte I. [1], Guenin E. [1], Lidgi-Guigui N. [1], Colas Florent [2], Ibrahim J. [3], Toury T. [3], Lamy de la Chapelle M. [1, *]

[1] Univ Paris 13, Sorbonne Paris Cite, Lab CSPBAT, CNRS,UMR7244, 74 Rue Marcel Cachin, F-93017 Bobigny, France.
[2] IFREMER, Ctr Brest, Interfaces & Sensors & Grp, BP 70, F-29280 Plouzane, France.
[3] Univ Technol Troyes, Lab Nanotechnol & Instrumentat Opt, Inst Charles Delaunay, FRE 2848, 12 Rue Marie Curie, F-10004 Troyes, France.

* Corresponding author : M. Lamy de la Chapelle,
email address : marc.lamydelachapelle@univ-paris13.fr

Abstract :

Nanoplasmonics is a growing field of optical condensed matter science dedicated to optical phenomena at the nanoscale level in metal systems. Extensive research on noble metallic nanoparticles (NPs) has emerged within the last two decades due to their ability to keep the optical energy concentrated in the vicinity of NPs, in particular, the ability to create optical near-field enhancement followed by heat generation. We have exploited these properties in order to induce a localised “click” reaction in the vicinity of gold nanostructures under unfavourable experimental conditions. We demonstrate that this reaction can be controlled by the plasmonic properties of the nanostructures and we propose two physical mechanisms to interpret the observed plasmonic tuning of the “click” chemistry.

Introduction

Nanoplasmonic effects are governed by coherent oscillations of the free electron gas of metal nanoparticles (NPs) at the incident electric field frequency. The excitation of these modes, called localized surface plasmons (LSP)[2,3], can be further enhanced if the frequency of the incoming light matches the LSP resonance (LSPR) frequency[4]. The unique optical properties of the metal NPs induced by LSP excitation are of great interest in the fields of physics[5,6] and biology[7,8]. It may also be exploited in chemistry[9]. This latter field can significantly benefit from the application of nanoplasmonics as an efficient source of electrons, light and heat. The control of chemical reactions at the metallic surfaces is a crucial parameter for many applications. For instance, a two-photon photopolymerization of a thin photo-resist layer SU8 has been achieved locally inside the nanogaps between lithographic gold nanostructures due to the near-field enhancement induced by LSP excitation[10]. Galloway *et al.* have also demonstrated light assisted protein immobilization in the nanogap between two gold nanoantennae within a nanometric accuracy[11]. In their study, the authors exploited the cleavage of disulfide bridges in the proteins resulting in their subsequent attachment to the gold nanoantennae in the regions of the highest near-field enhancement. Another important parameter to control the speed and yield of chemical reactions is the temperature generated by LSP. Thermoplasmonics is a recent field of research, which has proved to be highly applicable for many chemical approaches. Cao *et al.* have used the local heat generated by metallic NP through laser illumination to control the position and growth direction of a single semiconductor nanowire[12].

In this paper, we demonstrate that the plasmonic properties of metallic NPs can be exploited to induce “click” chemistry reactions. Introduced less than two decades ago, this set of reactions is described as simple, widely scoped, modular, generating high yields, and producing only harmless byproducts that can be isolated by non-chromatographic methods[13]. In particular, a copper-catalysed azide/alkyne click reaction has received considerable attention in organic and polymer chemistry[14] but also in nanosurface chemistry[15]. Another reaction: thiol-ene coupling, fulfills the click chemistry concept as well. This reaction known for over 100 years[16] and recently rediscovered[13], consists in grafting thiol-bearing molecules to a carbon double bond. The applications of this reaction have had significant impact in polymer synthesis and material science[17,18] and has attracted growing interest in surface functionalisation and modifications[19,20]. Generally, this reaction is performed through UV light or thermal activation, with the presence of a radical initiator.

In this contribution, we demonstrate that the thiol-ene coupling can be simply initiated in the visible range using nanoplasmonic effects. The kinetics of this reaction was monitored *in situ* by Surface Enhanced Raman Scattering (SERS). By investigating the reaction rates on different diameters of gold nanocylinders (NCs) made by electron-beam lithography (EBL) we claim that this reaction can be tuned by controlling the NCs plasmonic properties.

Experimental

Materials

2,2'-azobis(2-methylpropionamidine) dihydrochloride (AAPH, 97%), 2-mercaptoethanol (BME, 99%), ethanol (99.8%), 4-pentenoyl chloride (98%), 4-nitroaniline (99%), 1,4-butanedithiol (97%) and thiophenol (thiophenol, 99%) were purchased from Sigma-Aldrich (France) and allyl mercaptane (2-propene-1-thiol, 70%) was obtained from Acros Organic (France). All reagents were used without further purification. Deionized water with resistance of 18.2 MΩ.cm was used in all described experiments as the reaction medium.

SERS active substrates

Gold nano-cylinder (NCs) arrays on glass produced by electron beam lithography and lift-off techniques[34,35] were used for this study. The substrates were designed to contain the variable diameters of NCs: 110 nm, 140 nm and 200 nm. The height of the cylinders was set at 60 nm evaporated on 3 nm of chromium for better gold adhesion on glass. The gap between two NCs was kept constant at 200 nm to avoid any effect of near-field coupling.

General procedure for chemical reactions on gold surface

Prior to each experiment, gold NCs were cleaned as follows: substrates were immersed in ethanol for 10 min, dried using nitrogen and treated by ozone under intense 185 nm and 254 nm ultraviolet light (PSD Standard UV-Ozone Cleaner, Novascan), ensuring the removal of organic contaminants. Substrates were then once again immersed in ethanol for 10 min, dried and investigated by Extinction and Surface Enhanced Raman Spectroscopies in aqueous conditions using the microscopic side with the mould (Carl Roth).

Thiophenol grafting by thiol-ene click chemistry

The substrate was incubated in allyl mercaptan solution of 0.08 M in ethanol for 12 hours ensuring self-assembled monolayer (SAM) like coating formation to block the gold surface. As-prepared gold NCs based substrate was then ready to be introduced to a reaction mixture containing thiophenol (0.25 mM) and AAPH (0.25 mM) dissolved in deionized water. The sample was placed on a microscopic slide where the mould was filled with 100 µL of reaction mixture. The thiol-ene click reaction was then monitored by SERS.

Experiment C1: Thiophenol interaction with allyl mercapthan functionalized gold NCs

The substrate was functionalized with allyl mercaptan and then placed on a microscopic slide containing 100 µL of aqueous thiophenol solution (0.25 mM). Contrary to the experiment above, the radical initiator was not included here. Thiophenol interaction with double bonds decorated surface was then monitored by SERS.

Experiment C2: thiophenol interaction with mercaptoethanol functionalized gold NCs

The substrate was incubated in mercaptoethanol solution of 0.1 M in ethanol for 12 hours to block the free gold surface. The functionalized substrate was then orientated onto a microscopic slide with a mould filled with 100 µL of the aqueous solution containing thiophenol (0.25 mM) and AAPH (0.25 mM). Thiophenol interaction with mercapthoetanol was then monitored by SERS.

Experiment C3: thiophenol interaction with non-functionalized gold NCs

The cleaned substrate with gold NCs arrays was directly placed on a microscopic slide with the mould filled with 100 µL of solution containing thiophenol (0.25 mM) and AAPH (0.25 mM) in deionized water. Thiophenol interaction with non-functionalized gold surface was then monitored by SERS.

Pentenoyl-nitroaniline interaction with butanedithiol functionalized gold NCs

The substrate was first functionalized using butanedithiol (10 mM in ethanol) by incubating it in solution for 12 h. The substrate was then washed with ethanol and placed on a microscopic slide containing 100 µL of aqueous solution with dissolved pentenoyl-nitroaniline (0.2 mM) and AAPH (0.2 mM). Pentenoyl-nitroaniline was chemically synthesized from 4-pentenoyl chloride and 4-nitroaniline, using a nucleophilic addition reaction. As in the experiments above, molecular grafting by thiol-ene reaction was then monitored by SERS.

Raman spectroscopy measurements

SERS and extinction measurements were recorded using Xplora ONE (Horiba scientific) spectrometer. For SERS, a laser of 660 nm excitation wavelength with the power of 0.45 mW was focused on the sample with x60 objective (N.A. 0,70). Integration time for signal collection was set at 15s. Each spectrum was the average of two repetitive measurements. Applied grating of 600 grooves/mm ensured a spectral resolution of 3 cm^{-1}.

Nuclear Magnetic Resonance (NMR) measurements

Nuclear Magnetic Resonance (NMR) measurements were performed in deuterium oxide using Bruker Avance III 400 MHz instrument.

Results and discussion

Thiol-ene “click” reaction involves the addition of a thiol to an alkene group via a free-radical mechanism[21] (Figure 1).

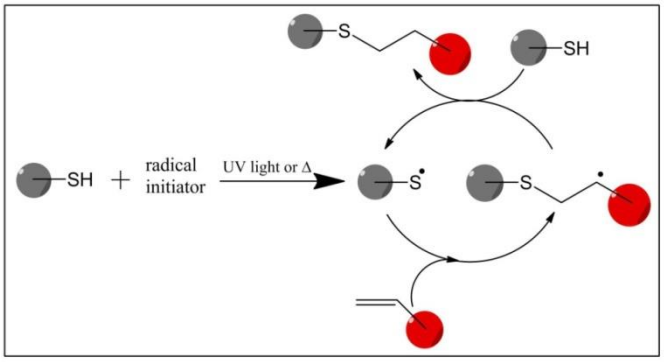

Figure 1: Schematic illustration of the free-radical thiol–ene coupling mechanism.

Briefly, in the initiation step the thiol group is converted to a thiyl radical thanks to the interaction with a photo or thermal radical initiator exposed to UV light[22,23] or to a specific temperature[24], respectively. This thiyl radical can then react with the C=C bond to form a carbon centred radical. From this step the initiation is turned to a propagation step resulting in the formation of a thio ether as a reaction product and a new thiyl radical subsequently involved in the reaction chain.

In our case, the click reaction was performed using 2,2’-Azobis(2-methylpropionamidine)dihydrochloride (AAPH) as radical initiator, allyl mercaptan as double bond substrate and thiophenol as reactant. The AAPH is known to be decomposed into cationic radicals under UV light (365 nm) or temperature above 60 °C (See supplementary information). The reaction was initiated at the surface of the gold NCs (figure 2a) in aqueous environment and using a 660 nm laser beam (figure 2b). The allyl mercaptan was grafted onto the NCs surface through the S-Au bond whereas the AAPH and the thiophenol were free in solution (figure 2c).

Since EBL allows the fine control of the size and shape of the nanostructures at the nanometer scale, the substrates benefit from the reproducibility of both: LSPR position and SERS signal[25,26]. Arrays of NCs (figure 2d) with different diameters: 110, 140 and 200 nm were fabricated to investigate whether the thiol-ene click reaction can occur due to plasmonic effects.

As shown by the extinction spectra of the NCs in aqueous environment (figure 2e), the 110 nm diameter NCs were found to have a LSPR position close to 660 nm (excitation laser wavelength) whereas 140 nm NCs had a LSPR position red-shifted compared to 660 nm. For the 200 nm NCs, the excitation wavelength was nearly out of resonance, resulting in a largely less intense electromagnetic near-field.

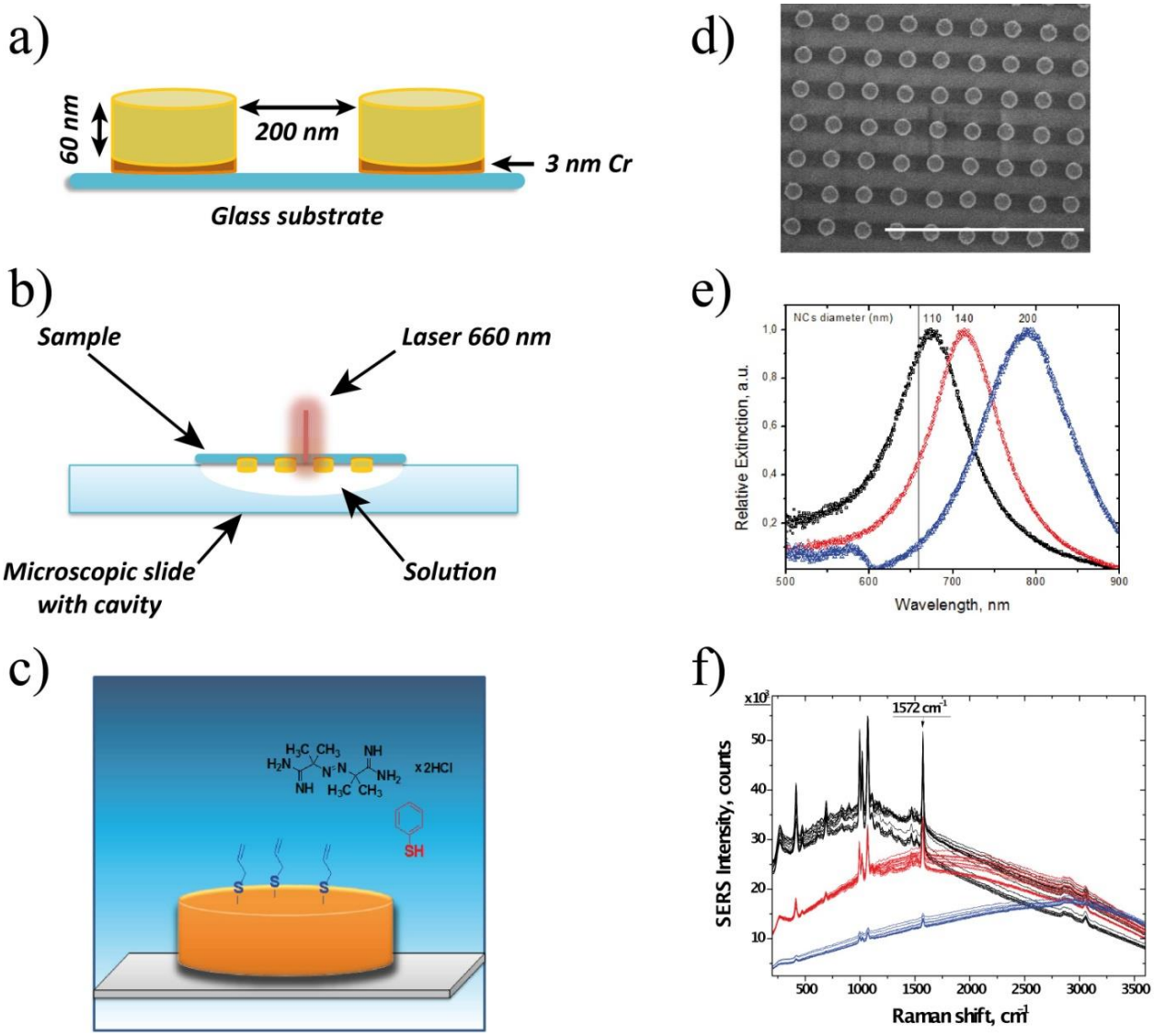

Figure 2: a) Schema of the nanocylinders (NCs) used in the experiments. b) Schema of the experimental configuration. c) Schema of the thiol-ene reaction configuration. d) Scanning electron microscopy image of an array of NCs with a diameter of 200 nm. e) Extinction spectroscopy measurements on 110 nm (black curve), 140 nm (red curve) and 200 nm (blue curve) NCs arrays. The grey line indicates the laser wavelength used for thiol-ene reaction initiation and SERS investigation. f) SERS spectra of grafted thiophenol onto gold NCs of 110 nm (black spectra), 140 nm (red spectra) and 200 nm (blue spectra) diameter.

The reaction kinetics were evaluated for the three diameters in order to observe changes in reaction performances depending on the mismatch between the LSPR position and the laser wavelength.

***In situ* thiol-ene click reaction**

To initiate the reaction, the solution of AAPH and thiophenol was deposited on a microscopic slide with a cavity and the substrate with NCs decorated with grafted allyl mercaptan was then placed above the slide with the NCs inside the solution. Local reaction at the microscale level was implemented using the excitation laser focused with a 60x objective (N.A. 0.70) through the NCs substrate. The reaction kinetics were then monitored by SERS in real time using the same laser wavelength. SERS spectra were first recorded on the 110 nm NCs: one spectrum each minute for a total duration of 30 min. The process was then reproduced on the NCs of 140 nm and finally on the NCs of 200 nm (figure 2f).

The peaks observed in the SERS spectra correspond to the thiophenol vibrations. Due to method limitations (including placing the substrate in liquid and laser focusing procedures) the NCs were exposed to the solution for about 4 min before the first SERS measurement was made. For this reason the SERS signal of thiophenol was not strictly equal to zero on the first SERS spectrum indicating a spontaneous thiophenol interaction with non-blocked gold areas. To follow the reaction kinetics, the intensity of the peak at 1572 cm^{-1} assigned to an aromatic C=C vibration was plotted versus reaction time (figure 3a) for all NCs diameters. The observed SERS intensity of the

thiophenol increases and reaches a plateau, when the gold surface is saturated. Reaction times of less than 10 min were observed for the 110 nm and the 140 nm diameters whereas for the 200 nm, saturation was not achieved even after 40 min of reaction. 10 min is very fast for this thiol-ene reaction since it has been estimated to be of several hours in normal conditions (*i.e.* without NCs and with UV excitation)[27]. To determine precisely the reaction time, the experimental data were fitted with a first order Langmuir isotherm assuming that during the reaction a single layer of thiophenol was formed:

$$\theta = \theta_{sat}\left[1 - \exp^{\left(-\frac{t}{\tau}\right)}\right] \qquad (1)$$

where θ is the surface coverage, θ_{sat} is the coverage saturation, t is the time and τ is the reaction time constant. Figure 3b shows the reaction time constant, τ, that corresponds to the time required to reach 63% of SERS signal saturation versus the shift between the LSPR position of NCs and the laser excitation wavelength, $\Delta\lambda=\lambda_{LSPR}-\lambda_{exc}$.

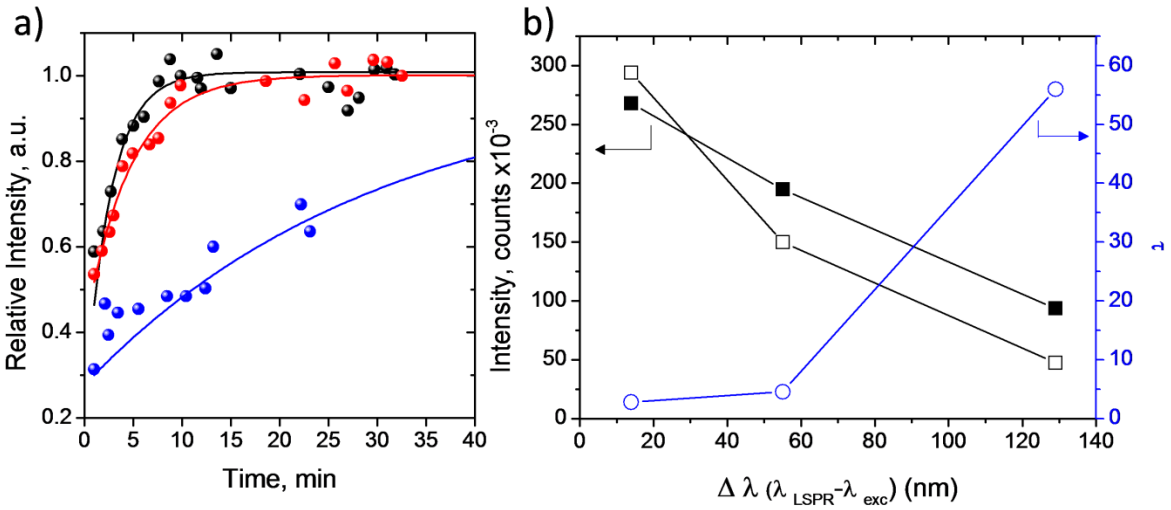

Figure 3: a) Relative SERS intensities of the integrated peak at 1572 cm^{-1} versus reaction time for the 110 nm (black dot), 140 nm (red dot) and 200 nm (blue dot) NCs. Solid lines correspond to the fitting of the experimental points using the equation (1) (110 nm: black line, 140 nm: red line and 200 nm: blue line). b) Absolute SERS intensity at saturation and reaction time plotted versus the mismatch between the LSPR position of NCs and the laser excitation wavelength. Hollow dot: reaction time for the 110 nm, 140 nm and 200 nm NCs. Hollow square: absolute SERS intensities of the thiophenol measured on the 110 nm, 140 nm and 200 nm NCs for the thiol-ene reaction after surface saturation. Plain square: absolute SERS intensities of the thiophenol measured on the 110 nm, 140 nm and 200 nm NCs for the experiment C3 and after surface saturation.

It is clearly visible, that the reaction time is strongly dependent on the LSPR position. A twenty times faster reaction was observed on highly resonant 110 nm NCs compared to 200 nm NCs. Unexpectedly, 140 nm NCs with a 54 nm difference between the LSPR position and the excitation wavelength reveals a slightly lower reaction efficiency compared to the one measured on 110 nm NCs.

In order to demonstrate that our experiments actually correspond to the thiol-ene "click" chemistry, the experimental conditions were modified to perform negative controls, since the grafting of thiophenol on the NCs can be attributed to two other mechanisms: spontaneous grafting or competitive replacement. On one hand, it is known that short molecules with the thiol group - like allyl mercaptan - form non-homogeneous self-assembled monolayers (SAM) due to the lack of intermolecular interactions[28]. This leaves non-blocked active gold sites for spontaneous thiophenol grafting. On the other hand, competitive molecular displacement could occur directly on the gold surface, inducing the replacement of allyl mercaptan by thiophenol[29]. Thus, the SERS signal measured in the thiol-ene experiments could then also include contributions from these two thiophenol-gold interactions. For this concern, three negative controls (experiments C1 to C3) were designed to analyze the thiophenol grafting rate *via* side reactions (figure 4). The first negative control (experiment C1) was designed to duplicate the thiol-ene reaction without a radical initiator. The second negative control (experiment C2) was dedicated to observe the competitive thiophenol adsorption by replacing molecules grafted onto the gold surface. Herein, mercaptoethanol was used instead of allyl mercaptan to avoid any reaction between thiophenol and the allyl group. The last negative control was devoted to the monitoring of the spontaneous adsorption of thiophenol on non-functionalized NCs (experiment C3). All these experiments were performed in the same manner as previously described for the thiol-ene reaction. The reaction kinetics of the three negative controls recorded on the 110 nm NCs are shown in figure 4 and are compared to the kinetics of the thiol-ene reaction.

The SERS signal for the experiments C1 and C2 are nearly constant with time. This suggests that in the latter experimental conditions, thiophenol was interacting spontaneously by replacing the short thiols previously deposited on the surface. Since this mechanism is a competitive one, equilibrium was reached very rapidly (less than a few minutes) resulting in a constant SERS signal.

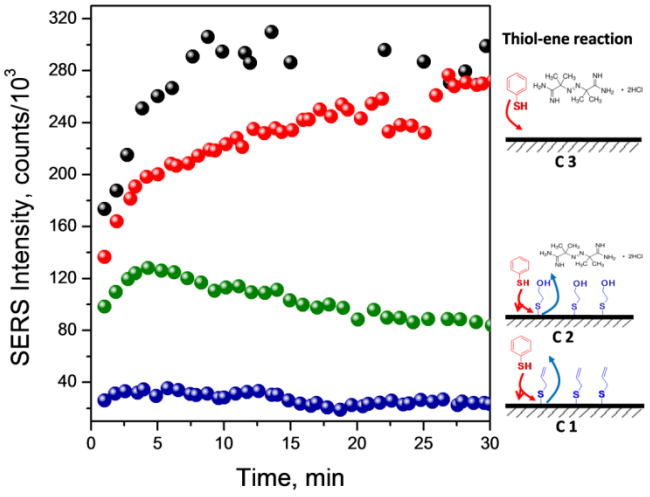

Figure 4: SERS intensities of the integrated peak at 1572 cm^{-1} for the thiol-ene reaction and for all three negative controls recorded on 110 nm NCs (black dot: thiol-ene reaction, blue dots: C1 negative control, green dots: C2 negative control, red dots: C3 negative control). The schemas of the different reactions are given on the right of each curve.

However, the measured signal is significantly lower than the one recorded during the thiol-ene reaction, meaning that the high level of the thiophenol signal observed with the thiolene reaction cannot be explained by a simple competitive mechanism. In fact, the non-zero SERS signal observed prior to the thiol-ene reaction start (figure 3a and figure 4 black circles) might be assigned to the competitive replacement mechanism. The fast increase in the SERS signal was then induced by the initiated thiol-ene reaction. Furthermore, the comparison of the thiol-ene reaction signal to the one achieved during experiment C1 suggests that AAPH is essential to initiate the thiol-ene reaction.

The SERS signal recorded in experiment C3 is relevant to the kinetics of thiophenol SAM formation. Two main observations can be made from the comparison between the experiment C3 and the thiol-ene reaction. Firstly, thiol-ene kinetics is faster than the spontaneous grafting of thiophenol suggesting the strong contribution of the “click” chemistry process. Secondly, the signal at saturation in experiment C3 is comparable to the one observed in the thiol-ene reaction. This means that the same NCs coverage has been achieved using either the thiol-ene or the simple thiol reaction.

By comparing the different reaction kinetics associated with each negative control experiment (C1 to C3), it is evident that thiophenol grafting onto NCs under conditions demonstrated in figure 3 is favored by the thiol-ene “click” reaction acting as a dominant mechanism.

The contribution of plasmon to the thiol-ene reaction can then be elaborated. To provide evidence, we compared the SERS intensities obtained after surface saturation for the thiol-ene reaction and for experiment C3 on the three NCs diameters (figure 3b). During experiment C3, the grafting of thiophenol should not be dependent on the plasmonic properties of the NCs since the thiol reaction with gold is not thermally or optically activated. The SERS signal ratio between NCs diameters observed in this experiment is thus only due to the effect of the LSPR position compared to the excitation wavelength[30] and does not reflect the modification in the coverage rate of the thiophenol on the NCs with different diameters. As expected for experiment C3, the ratio between SERS signal on 110 nm NCs is 2.5 larger than the one measured on the 200 nm due to plasmonic effects on the SERS signal. In the case of the thiol-ene reaction, this ratio is much higher, close to 6. Such a large ratio can only be explained by the higher efficiency of the thiol-ene reaction in thiophenol grafting. Thus, when the LSPR is shifted relative to the excitation wavelength, the thiol-ene reaction is less efficient whereas it is enhanced when the LSPR is close to the excitation wavelength. This is clear evidence that radical reaction is induced and can be tuned by the plasmonic properties of the NCs.

Plasmonic mechanisms

Thanks to NMR experiments (see supplementary information), we have demonstrated that the thiol-ene reaction monitored herein on the plasmonic substrates cannot be initiated at 660 nm wavelength without the plasmonic substrates. In a conventional thiol-ene experiment either a UV or a thermal activation is necessary to initiate the

reaction, even if this latter effect seems to be less efficient (see supplementary information). Thus, we propose two processes related to the plasmonic properties of the NCs to interpret our results.

The first one, which we call the photonic process, is related to the optical excitation of the radical initiator. It is known that when a molecule is in the close vicinity of a metallic surface its electronic levels are broadened as illustrated in figure 5a[31,32]. Electronic transitions can then occur at wavelengths outside the UV range whereas they are forbidden for the same molecules in solution and without metal. Through this process, the radical can be formed under initiation with a 660 nm wavelength. As the electromagnetic near-field is enhanced when the LSPR is close to the excitation wavelength, the formation of the radical should be favored as well. As a consequence, the reaction rate is highly improved on resonant NCs.

The second contributing mechanism is related to a thermal process. Discrete Dipole Approximation (DDA) calculations were performed to determine the near-field at the vicinity of the NCs surface (see supplementary information) and the increase in temperature around the NCs was then derived (figure 5b)[33]. Though an increase in temperature was obtained for all diameters it was found to be strongly dependent on the LSPR shift relative to the excitation wavelength. Nearly the same increase in temperature was calculated for 110 nm and 140 nm NCs, close to 50-55°C, whereas it was close to 15°C for 200 nm NCs. The attained temperatures were then high enough to induce the formation of the radical (70-75°C for the 110 and 140 nm NCs and 35°C for the 200 nm NCs).

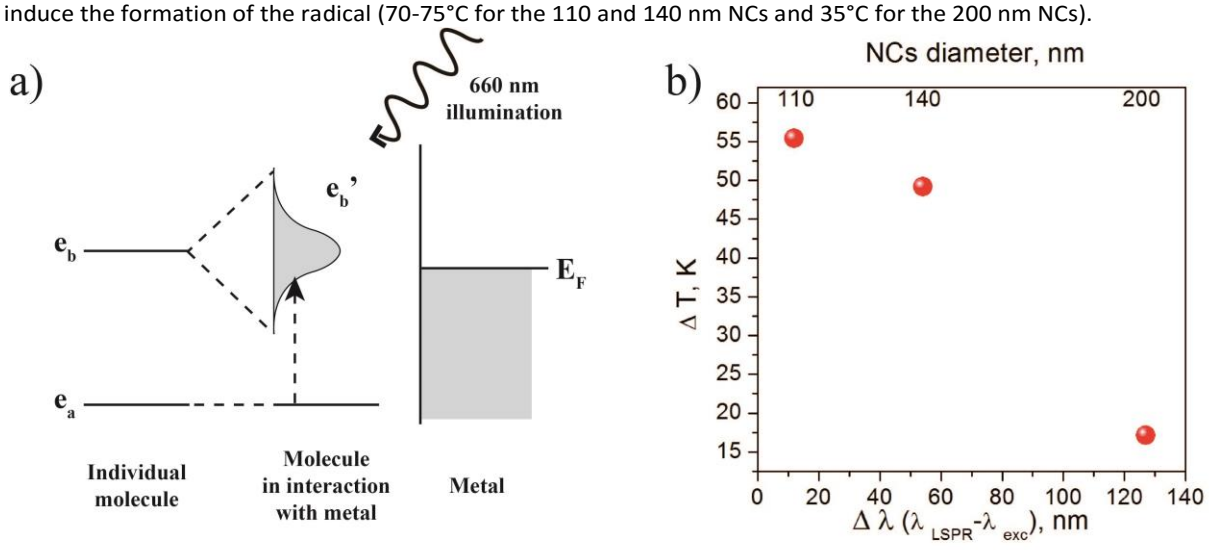

Figure 5: a) Schema of the photonic mechanism. On the left, the electronic configuration of an individual molecule with two levels (e_a and e_b) is represented. On the right, the same molecule is shown but in interaction with a metallic surface. The upper electronic level of the molecule is then broadened (e_b' in the middle schema) due to the interaction with the metallic electronic states (right schema with E_F the Fermi level). The dotted arrow in the middle schema represents the excitation of the molecule through the 660 nm illumination. b) Temperature increases plotted versus the mismatch between LSPR position of NCs and the laser excitation wavelength on the 110 nm, 140 nm and 200 nm NCs. The temperature increases were calculated using Discrete Dipole Approximation method.

he LSPR dependency on the kinetics (figure 3b) can be explained by such LSPR dependency on the temperature. Comparing plots in figures 3b and 5b, one can notice that the slope of the temperature curve is opposite to the one of the reaction time constant, τ. More precisely, the temperature increase induced around the 110 and 140 nm NCs accelerates the speed of the thiol-ene coupling reaction, while a lower temperature increase found in the 200 nm NCs results in a rather slow reaction rate.

We assume that both processes, thermal and photonic, are taking place since they are directly related to the plasmonic properties of the NCs. Both processes contribute simultaneously to the enhancement of the thiol-ene reaction efficiency.

To confirm this conclusion and to further improve thiol-ene reaction localisation, we set up one last experiment. To do this we performed an experiment contrary to the one carried out previously (Figure 2c). In this case, the thiol groups (butanedithiol) were grafted onto the 110 nm NCs surface whereas the molecules consisting in alkene function (pentenoyl-nitroaniline) and AAPH were dispersed in solution (figure 6a). As demonstrated in figure 6c, the reaction measured on three different points was working by means of a few minutes (measured from 2.1 to 7.9 minutes). Similar behaviour was observed for all recorded spots and the reaction was reproducible from one point to another. These results confirm that in this configuration the radical formed on the thiol group is only present at the focal point. In previous experiments (allyl mercaptan grafted on the surface), the radicals were formed on the thiophenol in the solution and then the initiation of the thiol-ene reaction outside the laser spot could not be

excluded. In the present experiment, the thiol-ene reaction could only occur locally inside the laser spot where the thiol groups were grafted. Accordingly, the reaction was limited to the laser spot and thus was highly localised. This paves the way to a quick and easy method to localise surface functionalisation via the "click" process at the nanometer scale through plasmonic effects.

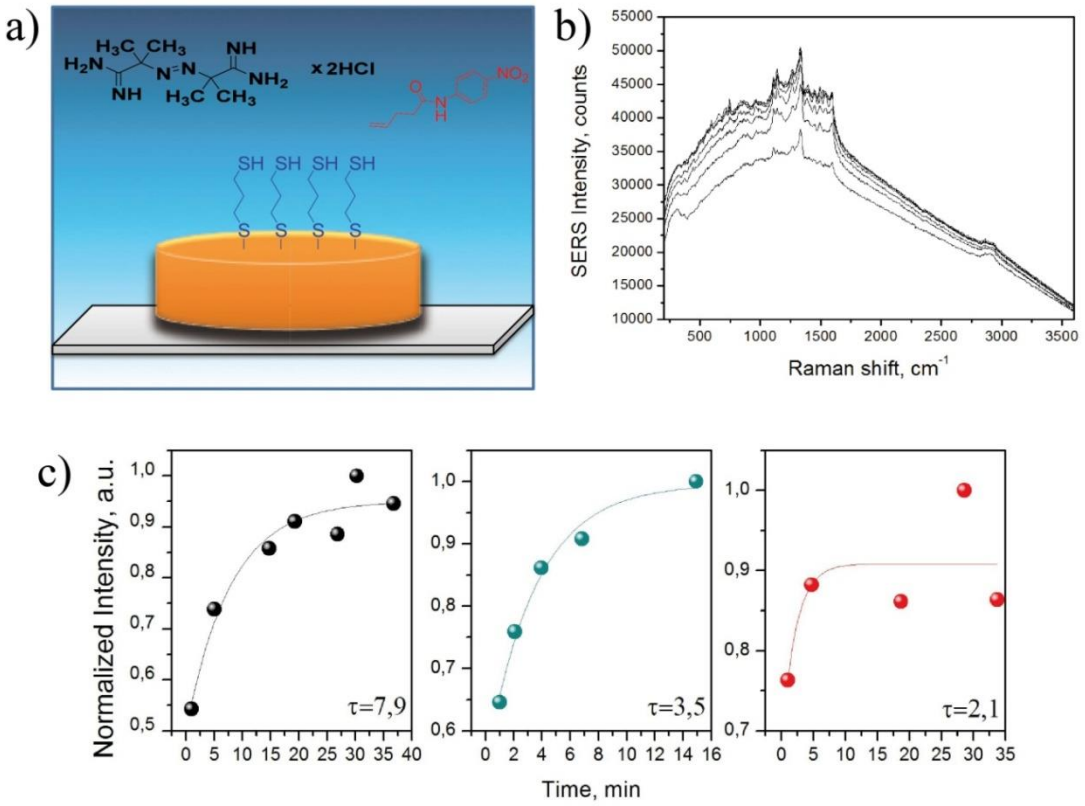

Figure 6: a) Schema of the thiol-ene reaction configuration. b) SERS spectra of grafted pentenoyl-nitroaniline to 110 nm NCs. c) Relative SERS intensities of the integrated peak at 1332 cm^{-1} versus reaction time for three different points on the SERS substrate. The solid lines correspond to the fitting of the experimental points using the equation (1). The reaction time constant, τ, in minutes is given in insert for each point.

Conclusions

We have demonstrated that the thiol-ene reaction can be induced at the surface of gold NCs even if the experimental conditions are not favourable, through the exploitation of the plasmonic properties of the nanostructures. These experiments demonstrate that the thiol-ene reaction can be performed in a few minutes and that by tuning the LSPR position we are able to control the kinetics of the reaction as well as the reaction localisation. This effect interpreted as the combination of both photonic and thermal effects can be used to enhance and control chemical reactions at the nanoscale level. To investigate the reaction mechanism and to have a better understanding on the nanoplasmonic effects, further experiments can be done involving different thiols and alkenes compounds as well as different radical initiators. Moreover, the careful selection of nanoparticles pursuing different plasmonic properties could also be meaningful to determine which process, thermal or photonic ones, is the dominant effect causing the initiation of thio-lene reaction.

Acknowledgements

The authors want to acknowledge the REMANTAS ANR project (ANR-11-ECOT-0010) for financial support.

References

1. M. I. Stockman, *Opt Express*, 2011, **19**, 22029-22106.
2. D. Bohm and D. Pines, *Physical Review*, 1951, **82**, 625-634.

3. R. H. Ritchie, *Physical Review*, 1957, **106**, 874-881.
4. E. Petryayeva and U. J. Krull, *Anal. Chim. Acta*, 2011, **706**, 8-24.
5. M. Pelton, J. Aizpurua and G. Bryant, *Laser & Photonics Reviews*, 2008, **2**, 136-159.
6. G. Volpe, M. Noack, S. S. Aćimović, C. Reinhardt and R. Quidant, *Nano Lett.*, 2012, **12**, 4864-4868.
7. A. S. Urban, T. Pfeiffer, M. Fedoruk, A. A. Lutich and J. Feldmann, *ACS Nano*, 2011, **5**, 3585-3590.
8. M. P. Raphael, J. A. Christodoulides, S. P. Mulvaney, M. M. Miller, J. P. Long and J. M. Byers, *Anal. Chem.*, 2011, **84**, 1367-1373.
9. G. Baffou and R. Quidant, *Chem. Soc. Rev.*, 2014, **43**, 3898-3907.
10. K. Ueno, S. Juodkazis, T. Shibuya, Y. Yokota, V. Mizeikis, K. Sasaki and H. Misawa, *J. Am. Chem. Soc.*, 2008, **130**, 6928-6929.
11. C. M. Galloway, M. P. Kreuzer, S. S. Aćimović, G. Volpe, M. Correia, S. B. Petersen, M. T. Neves-Petersen and R. Quidant, *Nano Lett.*, 2013, **13**, 4299-4304.
12. L. Cao, D. N. Barsic, A. R. Guichard and M. L. Brongersma, *Nano Lett.*, 2007, **7**, 3523-3527.
13. H. C. Kolb, M. G. Finn and K. B. Sharpless, *Angew. Chem. Int. Ed.*, 2001, **40**, 2004-2021.
14. M. Meldal and C. W. Tornøe, *Chem. Rev.*, 2008, **108**, 2952-3015.
15. N. Li and W. H. Binder, *J. Mater. Chem.*, 2011, **21**, 16717-16734.
16. T. Posner, *Berichte der deutschen chemischen Gesellschaft*, 1905, **38**, 646-657.
17. A. B. Lowe, *Polymer Chemistry*, 2010, **1**, 17-36.
18. A. B. Lowe, *Polymer Chemistry*, 2014, **5**, 4820-4870.
19. X. Han, C. Wu and S. Sun, *Appl. Surf. Sci.*, 2012, **258**, 5153-5156.
20. E. Lallana, A. Sousa-Herves, F. Fernandez-Trillo, R. Riguera and E. Fernandez-Megia, *Pharm. Res.*, 2012, **29**, 1-34.
21. K. Griesbaum, *Angewandte Chemie International Edition in English*, 1970, **9**, 273-287.
22. V. S. Khire, A. M. Kloxin, C. L. Couch, K. S. Anseth and C. N. Bowman, *J. Polym. Sci., Part A: Polym. Chem.*, 2008, **46**, 6896-6906.
23. P. Jonkheijm, D. Weinrich, M. Köhn, H. Engelkamp, P. C. M. Christianen, J. Kuhlmann, J. C. Maan, D. Nüsse, H. Schroeder, R. Wacker, R. Breinbauer, C. M. Niemeyer and H. Waldmann, *Angew. Chem. Int. Ed.*, 2008, **47**, 4421-4424.
24. D. Dupin, A. Schmid, J. A. Balmer and S. P. Armes, *Langmuir*, 2007, **23**, 11812-11818.
25. N. Guillot and M. Lamy de la Chapelle, *Journal of Nanophotonics*, 2012, **6**, 064506.
26. J. N. Anker, W. P. Hall, O. Lyandres, N. C. Shah, J. Zhao and R. P. Van Duyne, *Nat Mater*, 2008, **7**, 442-453.
27. B. H. Northrop and R. N. Coffey, *J. Am. Chem. Soc.*, 2012, **134**, 13804-13817.
28. Chi, J. Zhang and J. Ulstrup, *The Journal of Physical Chemistry B*, 2006, **110**, 1102-1106.
29. T. Kakiuchi, K. Sato, M. Iida, D. Hobara, S.-i. Imabayashi and K. Niki, *Langmuir*, 2000, **16**, 7238-7244.
30. N. Guillot and M. L. de la Chapelle, *J. Quant. Spectrosc. Radiat. Transfer*, 2012, **113**, 2321-2333.
31. T. E. Furtak and J. Reyes, *Surf. Sci.*, 1980, **93**, 351-382.
32. J. I. Gersten, R. L. Birke and J. R. Lombardi, *Phys. Rev. Lett.*, 1979, **43**, 147-150.
33. G. Baffou, P. Berto, E. Bermúdez Ureña, R. Quidant, S. Monneret, J. Polleux and H. Rigneault, *ACS Nano*, 2013, **7**, 6478-6488.
34. J. Grand, S. Kostcheev, J. L. Bijeon, M. L. de la Chapelle, P. M. Adam, A. Rumyantseva, G. Lérondel and P. Royer, *Synth. Met.*, 2003, **139**, 621-624.
35. J. Grand, M. L. de la Chapelle, J. L. Bijeon, P. M. Adam, A. Vial and P. Royer, *Physical Review B*, 2005, **72**, 033407.